Capillary RheoSANS: Measuring the rheology and nanostructure of complex fluids at high shear rates

Ryan P. Murphy,[1] Zachary W. Riedel,[1] Marshall A. Nakatani,[1] Paul F. Salipante,[2] Javen S. Weston,[3] Steven D. Hudson,[2] and Katie M. Weigandt[1]

[1] *NIST Center for Neutron Research, National Institute of Standards and Technology Gaithersburg, Maryland, USA*

[2] *Materials Science and Engineering Division, National Institute of Standards and Technology Gaithersburg, Maryland, USA*

[3] *Russell School of Chemical Engineering, University of Tulsa, Tulsa, Oklahoma, USA*

(Dated: June 17, 2020)

ELECTRONIC SUPPLEMENTAL INFORMATION (ESI)

Commercial equipment and materials identified in this work do not imply recommendation nor endorsement by the National Institute of Standards and Technology.

Capillary RheoSANS setup

CRSANS can be operated in either (1) continuous, unidirectional flow or (2) reciprocating flow. Both setups use the same fused silica capillaries and tubing connections.

In the unidirectional flow setup, Dionex P-580 dual-piston pumps produce unidirectional, pressure-driven flow of the sample through the capillary, as shown in Fig 1. The dual-piston pumps have a minimum flow rate $Q_{min} = 0.001$ mL min^{-1}, a maximum flow rate $Q_{max} = 10$ mL min^{-1}, and maximum operating pressure $P_{max} = 500$ bar. Ultra-high molecular weight polyethylene (UHMWPE) pump seals are checked and replaced often with abrasive samples. Check valves located at the inlet and outlet of the first chamber prevent backwards flow of the sample. The sample fluid at the capillary outlet can be recycled to the pump feed such that the total sample volume remains small. The minimum feasible sample volume was ≈ 2 mL to ensure the pump feed tube remains submerged within the sample reservoir and to avoid air bubbles in the feed tubing. A high pressure dynamic mixer with magnetic stirring can be used to mix separate sample streams. High shear rates are not necessary for high-throughput contrast variation, and a 0.5 mm pathlength rectangular cell was used in place of the capillary coil to increase the scattering volume.

In the reciprocating flow setup, high pressure syringe pumps are used instead (Cetoni neMESYS syringe pumps). The syringe pumps equipped with a 3 mL stainless steel syringe have $Q_{min} = 4.4$ nL min^{-1}, $Q_{max} = 21$ mL min^{-1}, and $P_{max} = 510$ bar. The sample is pumped back and forth between the two syringe pumps, in which the flow direction is reversed after a specified injection volume. Pressure sensors are connected both at the capillary inlet and outlet. One advantage of reciprocating syringe pumps is that the sample does not contact atmosphere once it is purged and sealed. Therefore, reciprocating syringe pumps are suggested for volatile samples to limit evaporation.

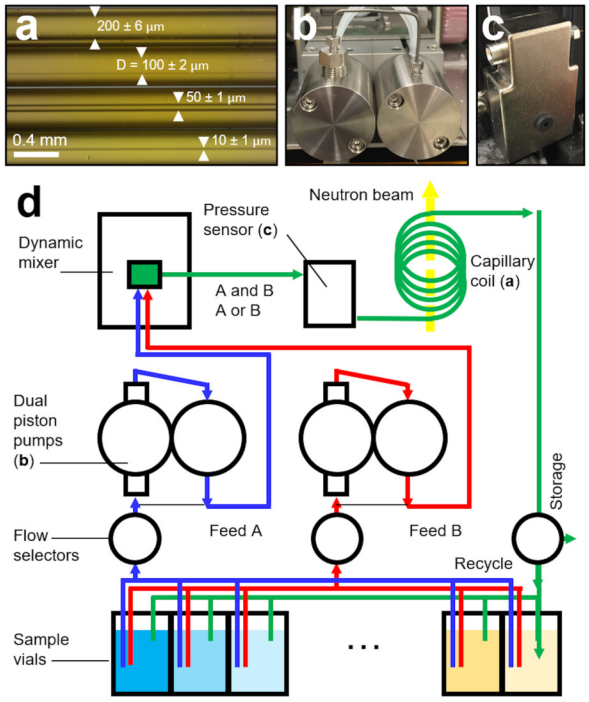

FIG. 1. (a) Fused silica capillaries used for CRSANS, with outer diameter of ≈ 360 μm and inner diameters D of 200, 100, 50, and 10 μm from top to bottom. (b) High-pressure, dual piston pumps used in continuous flow setup. (c) High-pressure, flow-through pressure sensors. (d) Flow schematic for two dual piston pumps connected to a dynamic mixer. This schematic was used for high-throughput contrast variation by varying the feed ratios and using a rectangular slit cell instead of a capillary to increase the scattering volume.

High-pressure flow through pressure sensors (DJ Instruments, DF2-High Pressure) were used to measure the pressure drop along the capillary (Fig. 1c). The capillary was directly connected to the pressure sensor using crimped PEEK fittings and 1/16 inch, 10-32 stainless steel compression fittings. Optional flow selector valves

can be implemented to quickly switch between different samples and capillary configurations.

Pressure calibrations

The pressure drop and flow rate of an incompressible, Newtonian fluid in a straight capillary or pipe is related by the Hagen-Poisuille equation,[1]

$$\Delta P = \frac{8\eta L Q}{\pi R^4} \tag{1}$$

in which ΔP is the pressure along the entire capillary length L, η is the solution viscosity, Q is the volumetric flow rate, and R is the inner radius of the capillary ($R = D/2$).

For Newtonian fluids, the average velocity is $v_{avg} = \Delta P R^2 (8\eta L)^{-1} = Q(\pi R^2)^{-1}$, and the maximum velocity evaluated at the capillary center ($r = 0$) is $v_{max} = 2v_{avg} = 2Q(\pi R^2)^{-1}$. The velocity profile along the z-axis $v(r)$ as a function of the distance r from the center is $v(r) = \Delta P R^2 (4\eta L)^{-1}(1 - (r/R)^2)$, which assumes a no-slip boundary condition ($v(r) = 0$ at $r = R$), and zero shear-rate at the center ($dv/dr = 0$ at $r = 0$).

To obtain a voltage-pressure calibration, a capillary with a measured L and D was loaded with pure water. As shown in Fig. 2a, the flow rate was increased at specified intervals, and the voltage from the pressure sensor was recorded at each flow rate for 60 s. Pulses in the voltage or pressure due to piston cycling are neglected from the averaging of the steady-state voltage ($\langle V_{ss} \rangle$). After extracting $\langle V_{ss} \rangle$ at each flow rate, a relationship between flow rate Q and the voltage is established, as shown in Fig. 2b. Note that the measured offset voltage ($V_{offset} = 0.5$ V) has been subtracted such that $\langle V_{ss} \rangle = 0$ at $Q = 0$. Using the Eq. 1 and the known variables $\eta = 1.00$ mPa-s at 20 °C, $L = 347$ mm, and $R = 99.5$ μm, the only remaining unknown variable is the scaling pre-factor to convert between voltage and pressure. For a Newtonian fluid, the slope of the best fit line in Fig. 2b (red solid line) is equal to $c8\eta L R^{-4}$, in which the pre-factor c is found by linear regression to be 3.38 ± 0.02 mV/bar.

Wall slip

For Newtonian fluids, the apparent shear rate evaluated at the capillary wall $\dot{\gamma}_w^a$ is given as,

$$\dot{\gamma}_w^a = \frac{4Q}{\pi R^3} = \frac{\Delta P R}{2\eta L} = \frac{2v_{max}}{R} \tag{2}$$

in which v_{max} is the maximum fluid velocity at the center line ($v_{max} = 2v_{avg}$).

The apparent shear rate at the wall is decreased if there is slip at the wall. Slip is typically characterized by a slip

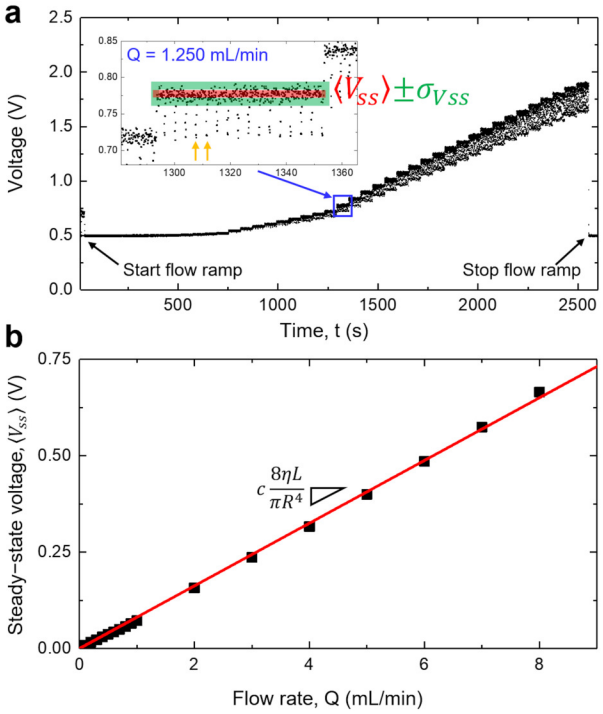

FIG. 2. (a) Raw voltage data obtained from the pressure sensor located at the capillary inlet as a function of time, in which the flow rate increases step-wise every 60 s. The inset shows the averaged steady-state voltage $\langle V_{ss} \rangle$ and one standard deviation σ_{Vss} extracted at a flow rate of $Q = 1.250$ mL min^{-1}. The voltage pulses (orange arrows in the inset) due to the piston cycling are neglected in the steady-state averaging. (b) The slope of the best-fit line between the steady-state flow rate Q and voltage $\langle V_{ss} \rangle$ is $8c\eta L/(\pi R^4)$. Since η, L, and R are known, this gives the unknown scaling pre-factor and calibration constant $c = 3.38 \pm 0.02$ mV/bar.

velocity v_{slip} along the direction of flow. The slip velocity can be determined by varying the capillary inner radius R using the Mooney analysis method given by,[1]

$$\dot{\gamma}_w^a = \frac{4Q}{\pi R^3} = \frac{4v_{slip}}{R} + \dot{\gamma}_w^c \tag{3}$$

in which $\dot{\gamma}_w^c$ is the slip-corrected shear rate. From Eq. 3, a plot of $4Q(\pi R^3)^{-1}$ as a function of R^{-1} gives a linear relationship between (1) the slip velocity $v_{slip} = m/4$ where m is the slope of the best-fit line, and (2) the slip-corrected apparent shear rate $\dot{\gamma}_w^c = b$ where b is the intercept of the best-fit line. This measurement is repeated for a range of pressure drops ΔP, radii R, and lengths L that have equivalent wall stress σ_w. Since CR-SANS currently controls flow rate only, measurements must be regrouped into the equivalent values of wall stress $\sigma_w = \Delta P R (2L)^{-1}$ for different capillary R and L. An example Mooney plot for pure water flowing through different capillaries is shown in Fig. 3a.

Once the slip velocity has been determined, Eq. 3 is rearranged for the slip-corrected shear rate $\dot{\gamma}_w^c$. For the

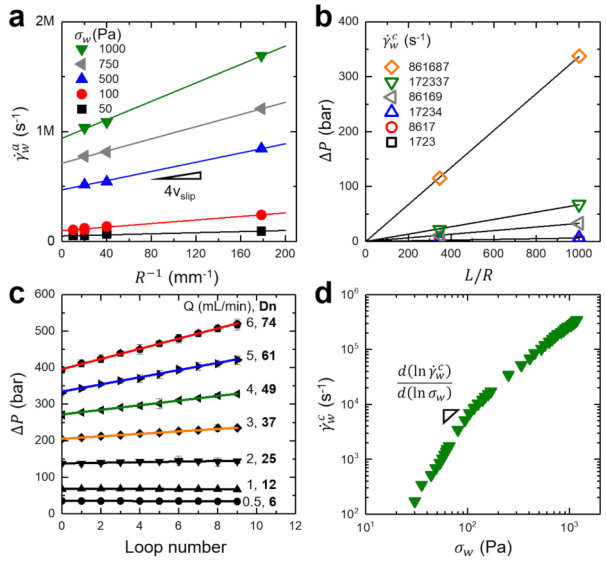

FIG. 3. (a) Mooney plot to determine the slip velocity v_{slip} using Eq. 3. (b) Bagley plot used to determine the additional pressure drop due to end effects $_{end}$ using Eq. 4. (c) Additional pressure drop effects due to wall curvature at sufficiently high flow rates and Dn number. (d) WR method to correct for non-parabolic flow profile and to estimate the true shear rate at the wall using Eq. 2. The sample used in (a-c) is pure water, while the sample in (d) is a worm-like micelle dispersion (4.6% SLES by mass in D_2O brine).

example in Fig. 3a, v_{slip} increases from approximately 0.06 m s^{-1} to 1.0 m s^{-1} with increasing wall stress and wall shear rate. A characteristic slip length l_s is defined based on the slip velocity and slip-corrected shear rate at the wall, $l_s = v_s/\dot{\gamma}_w^c$. If the slip length is assumed to be constant for a fixed fluid-solid surface boundary (water-silica), the average slip length is $l_s = 1.2 \pm 0.4$ μm. Notice that for measurements using capillaries with $D = 100$ μm or $R^{-1} = 20$ mm^{-1}, the shear rate correction due to wall slip is relatively small (3% to 9% change). However, for measurements using capillaries with $D = 11$ μm or $R^{-1} = 180$ mm^{-1}, the correction becomes even more significant (50% to 60% change).

Capillary end effects

An additional pressure drop contribution due to fluid entering or exiting the capillary can be significant, particularly for short capillaries or long entrance lengths.[2] To distinguish this end effect, the total pressure drop along the capillary ΔP is measured as a function of the aspect ratio L/R, given by[1]

$$\Delta P = 2\sigma_w \frac{L}{R} + P_{end} \tag{4}$$

in which σ_w is the shear stress at the wall and P_{end} is the pressure drop due to end effects at the entrance and exit. Using the Bagley method, measurements of the pressure drop are repeated for different L/R and slip-corrected shear rates $\dot{\gamma}_w^c$, as shown in Fig. 3b. The slope of the best-fit line is equal to $2\sigma_w$, while the intercept is equal to P_{end} at a specified $\dot{\gamma}_w^c$. For CRSANS, the pressure drop along the capillary length is large ($L/R > 100$) such that $P_{end} = 0$ with 95% confidence. Thus, end effects are neglected in this work. However, end effects may be significant with shorter capillaries ($L/R < 100$) and with complex fluids that exhibit large entrance lengths.[2]

Effects of wall curvature

For curved capillaries or pipes, an additional pressure drop contribution occurs from the bending of the capillary wall and the formation of secondary flows.[3] At low Dean numbers ($Dn < 30$), the effect of curvature is negligible. However, at larger Dean numbers ($Dn \gg 30$), the increasing magnitude of secondary flows can increase the pressure drop relative to a straight capillary.

The flexibility of the fused silica capillary enables a convenient experimental system to measure the additional pressure drop due to wall curvature. In Fig. 3c, the measured pressure drop for water is plotted as a function of the number of loops in the capillary coil, in which each loop bends a full 360 degrees to make a helical coil with diameter $D_c = 30$ mm and pitch equal to $OD = 360$ μm. Note that the minimum feasible coil diameter is approximately $D_c = 30$ mm, which is limited by the tensile stress generated at the outer diameter of the fused silica capillary. Since the same capillary is used to make coils with different loop numbers, the capillary $L = 1000$ mm and $D = 99.5$ μm remain identical. A straight capillary configuration corresponds to a loop number of 0 and an infinite coil diameter $D_c \to \infty$.

At lower flow rates $Q \leq 2$ mL min^{-1}, the additional pressure drop due to curvature is negligible, as given by the zero slope in the best-fit line (solid lines). However, as the flow rate increases to $Q2$ mL min^{-1}, the trend in ΔP vs. loop number remains linear, but the slope increases significantly with increasing flow rate. The transition at $Q \approx 3$ mL min^{-1} corresponds to $Dn \approx 37$, which is good agreement with other measurements when $D/D_c \ll 1$ and $Dn > 30$.[3]

The pressure drop for an effectively straight capillary can be estimated from a coiled capillary if the correlations between loop number, coil diameter, and flow rates are established as shown in Fig. 3c. However, flow instabilities that transition from the laminar flow regime to the turbulent flow regime will not necessarily occur at the same flow rates, since the onset for secondary flow instabilities are characterized by Dn (coiled capillary) instead of Re (straight capillary). Moreover, the dimensionless numbers Dn and Re do not account for viscoelastic effects of Non-Newtonian fluids, which could

cause an elasticity-driven instability that precedes the inertial-driven instability. Since the capillary can be easily coiled and uncoiled, it is recommend that the viscosity measurements of each sample be made both in a straight configuration and coiled configuration to establish if the effects of curvature are negligible or significant.

Non-Newtonian flow profiles

For non-Newtonian fluids, where η changes with varying $\dot{\gamma}$, the velocity profile can deviate from the parabolic profile for Newtonian fluids. The Weissenberg-Rabinowitsch (WR) correction can be applied to account for the non-parabolic flow profile and to approximate the true shear rate $\dot{\gamma}_w$ at the wall, given as[1]

$$\dot{\gamma}_w = \dot{\gamma}_w^c \left[\frac{1}{4} \left(3 + \frac{d \ln \dot{\gamma}_w^c}{d \ln \sigma_w} \right) \right] \tag{5}$$

in which $\dot{\gamma}_w^c$ is the slip-corrected shear rate (Eq. 3) and σ_w is the true shear stress at the wall corrected for end-effects (Eq. 4). An example of the WR correction analysis is shown in Fig. 3d for a shear-thinning suspension of worm-like micelles (4.6 % by mass). In this example, the capillary is straight with $D = 99.5$ μm and $L = 1000$ mm. The slope is evaluated between each point to estimate the derivative term $(d \ln \dot{\gamma}_w^c / d \ln \sigma_w)$ and to estimate the true shear rate near the wall $\dot{\gamma}_w$ using Eq. 5. In this case, the non-parabolic velocity tends to increase the shear rate near the wall and consequently decrease the shear rate near the center.

True viscosity

After accounting for the effects of wall slip, end effects, non-parabolic flow profiles, and curvature effects, the *true* viscosity of the complex fluid is given simply as the ratio of end-corrected shear stress σ_w and true shear rate at the wall $\dot{\gamma}_w$,

$$\eta(\dot{\gamma}_w) = \frac{\sigma_w}{\dot{\gamma}_w} \tag{6}$$

An example viscosity measurement protocol is as follows: (1) Measure the capillary radius R and length L. (2) Measure the calibrated steady-state voltage and calculate the pressure drop ΔP for a series of flow rates Q. (3) Apply the Mooney correction to determine the slip velocity and calculate the slip-corrected shear rate using Eq. 3. (4) If end effects are non-negligible, apply the Bagley correction to determine P_{end} and calculate the true shear stress at the wall at each flow rate using Eq. 4. (5) Estimate the true shear rate at the wall for a non-parabolic flow profile using the point-by-point Weissenberg-Rabinowitsch correction given in Eq. 5. (6) Calculate the true viscosity of the sample by the ratio of the corrected shear stress and corrected shear rate using Eq. 6.

Viscous heating effects

Significant viscous heat dissipation can occur at sufficiently high shear rate or high viscosity. Based on the steady-state heat generation due to viscous heating and heat loss due to conduction through the capillary wall, the steady-state increase in temperature ΔT due to viscous heating is estimated as,[2]

$$\Delta T \approx \frac{4 \eta v_{avg}^2 \ln (D_o / D)}{k_w} \tag{7}$$

in which ΔT is the increase in fluid temperature at steady-state relative to the ambient temperature, v_{avg} is the average fluid velocity, D_o is the outer diameter of the capillary, and k_w is the thermal conductivity of the wall material. Under the condition where $\eta = 1$ mPa-s, $Q = 10$ mL min^{-1}, $v_{avg} = 21$ m s^{-1}, $D = 100$ μm, $D_o = 360$ μm, and k_w=1.4 W m^{-1} K^{-1}, the increase in temperature is estimated to be $\Delta T \approx 1.6$ K. Thus, the effect of viscous heating is neglected in this work. From Eq. 7, the change in temperature is expected to scale as $\Delta T \sim \eta$ and $\Delta T \sim v_{avg}^2$, or equivalently $\Delta T \sim Q^2$ and $\Delta T \sim \dot{\gamma}_w^2$.

Sample preparation

Commercial equipment and materials identified in this work do not imply recommendation nor endorsement by the National Institute of Standards and Technology.

Silica nanoparticle suspensions were prepared by concentrating a stock suspension of silica dispersed in water (Ludox-TM50, 50 % by mass SiO_2, Sigma-Aldrich) by centrifugation at 10000 g, and then diluting with H_2O to 21% and 36% SiO_2 by volume. For contrast variation experiments, dilute silica suspensions were prepared by suspending the silica stock in H_2O at 1% SiO_2 by volume and in D_2O-rich solvent at 1% SiO_2 by volume (solvent composition of 97% by volume D_2O, 3% by volume H_2O). Different solvent compositions were mixed and injected into the sample cell using an in-line dynamic mixer and two dual piston pumps (ESI, Fig. 1d).

The monoclonal antibody solutions contained the NISTmAb reference material RM 8671 (NISTmAb, Humanized IgG1 Monoclonal Antibody, National Institute of Standards and Technology). A concentrated stock of NISTmAb was prepared in hydrogenated buffer (12.5 mmol/L L-histidine, 12.5 mmol/L L-histidine HCl, pH 6.0 in H_2O) at a mAb concentration of 100 mg mL^{-1}. This mAb stock was subsequently transferred to deuterated buffer by repeated centrifugation and purification

steps using a centrifuge filter with 50 kg mol^{-1} cutoff. The deuterated buffer contained the same salt concentrations with adjusted pH 6.0 in D_2O, i.e. pD $\approx$ 6.0 with small addition of NaOH in D_2O.[4] Protein concentration of the final solution was 25 mg mL^{-1}, as determined by UV spectroscopy.

Worm-like micelles (WLM) samples were prepared by mixing a stock solution of sodium lauryl ether sulfate (SLES, Stepan Company, trade name of Steol CS-460 with mass fractions of 60% SLES, 25% water, 15% ethanol, and a small amount of unsulfated fatty alcohols),[5] deuterium oxide (D_2O, Cambridge Isotope Laboratories, 99.8% D_2O by mass), and sodium chloride (NaCl, Fisher Scientific, $>$ 99 % NaCl by mass). The micelle mass fractions were varied from 1.2%, 2.3%, and 4.6% SLES by mass, while the salt concentration in D_2O was constant at 8% NaCl by mass for each sample. Samples were heated to 40 °C and sonicated in a bath sonicator until visibly clear and homogeneous.

[1] C. W. Macosko, *Rheology: Principles, Measurements, and Applications*, Wiley-VCH, Inc., 1994.

[2] P. F. Salipante, V. L. Dharmaraj and S. D. Hudson, *Journal of Rheology*, 2020, **64**, 481–492.

[3] S. A. Berger, L. Talbot and L. S. Yao, *Annu Rev Fluid Mech*, 1983, **15**, 461–512.

[4] A. Krezel and W. Bal, *J Inorg Biochem*, 2004, **98**, 161–6.

[5] J. S. Weston, D. P. Seeman, D. L. Blair, P. F. Salipante, S. D. Hudson and K. M. Weigandt, *Rheologica Acta*, 2018, **57**, 241–250.